Atmósfera 38, 129-149 (2024)
https://doi.org/10.20937/ATM.53226

El Niño-Southern Oscillation diversity and its relationship with the North Atlantic Oscillation – Atmospheric anomalies response over the North Atlantic and the Pacific

Gabriel Santiago GUTIÉRREZ-CÁRDENAS[1] and Diana Cristina DÍAZ[2]*

[1]*Centro Interdisciplinario de Ciencias Marinas, Instituto Politécnico Nacional, 23096 La Paz, Baja California, México.*
[2]*Departamento de Ciencias Básicas y Modelado, Universidad de Bogotá Jorge Tadeo Lozano, Bogotá D.C., 110821, Colombia.*
*Corresponding author: dianac.diaz@utadeo.edu.co

Received: September 20, 2022; Accepted: March 14, 2023

RESUMEN

Con el fin de explorar los impactos de El Niño-Oscilación del Sur (ENSO) sobre la Oscilación del Atlántico Norte (NAO), se investigó la correlación lineal entre los índices de cada oscilación. Los índices Niño 1+2, Niño 3, Niño 3.4, Niño 4, ONI, SOI, BEST, TNI y MEI se usaron para representar el ENSO, además del índice NAO. El análisis tiene en cuenta la diversidad del ENSO en su estructura espacial. Los resultados mostraron que, al omitir los años con eventos de La Niña del Pacífico Oriental, la correlación lineal aumentó con respecto a otros escenarios. Las respuestas de la NAO para el ENSO del Pacífico Central mostraron linealidad, mientras que para el ENSO del Pacífico Oriental ésta parece ser menor, lo cual explicaría por qué la relación ENSO/NAO ha sido difícil de identificar y predecir. La relación TNI-NAO tuvo los valores de correlación más altos, seguida de NAO-El Niño 4, en tanto que las relaciones NAO/El Niño 1+2 y NAO/El Niño 3 mostraron los coeficientes más bajos. Los resultados confirman que la dinámica atmosférica sobre el Atlántico Norte tiene una teleconexión mayor con el Pacífico Occidental y Central que con el Pacífico Oriental. Los cambios en la convección profunda, la circulación atmosférica y la vorticidad se discuten como posibles mecanismos que desencadenan los cambios en los impactos sobre el Atlántico Norte y otras regiones. Los mapas compuestos de anomalías evidencian el contraste en los efectos de ambos eventos y la importancia de considerar dichas diferencias al modelar la dinámica oceánica.

ABSTRACT

To explore the impacts of El Niño-Southern Oscillation (ENSO) on the North Atlantic Oscillation (NAO), the linear correlation among the indices of each oscillation was investigated. The indices Niño 1+2, Niño 3, Niño 3.4, Niño 4, ONI, SOI, BEST, TNI and MEI were used to represent the ENSO, besides the NAO index. The analysis considers the ENSO diversity in its spatial structure. The results show that when years with Eastern Pacific (EP) La Niña events were omitted, the linear correlation increased concerning other scenarios. This means that NAO responses for the Central Pacific (CP) ENSO tend to be linear, but seemingly they are not so for EP ENSO, which explains why the ENSO/NAO relationship has been difficult to identify and predict. The TNI-NAO relationship had the highest correlation values, followed by NAO-El Niño 4, whilst NAO/El Niño 1+2 and NAO/El Niño 3 showed the lowest coefficients. The results also confirmed that the atmospheric dynamics over the North Atlantic have a more linear teleconnection to the West and Central Pacific than to the Eastern Pacific. Changes in deep convection, atmospheric circulation, and vorticity are discussed like possible mechanisms that trigger the changes in impacts over the North Atlantic and other locations. The composite anomalies map also showed the contrast in the effects of both events and the importance of considering those differences when modeling ocean dynamics.

Keywords: CP ENSO, EP ENSO, teleconnections, ocean-atmosphere interaction.

1. Introduction

El Niño-Southern Oscillation (ENSO) is the result of the ocean-atmosphere interaction, which causes sea surface temperature (SST) positive and negative anomalies in the Central and Eastern Tropical Pacific and interannual variation of surface atmospheric pressure over the Tropical Indo-Pacific (Tedeschi et al., 2015). ENSO is one of the main sources of interannual climate variability on a planetary scale, and its effects in different parts of the world have been widely studied (Takahashi et al., 2011; Tedeschi et al., 2015; Du et al., 2020). One of the frequent findings is the diversity of anomalies that ENSO causes in variables such as air temperature and precipitation for a particular place (Díaz and Villegas, 2015; Mohammadi et al., 2020; Salas et al., 2020). This makes it difficult to predict and develop prevention plans for possible adverse consequences for the population. Furthermore, research carried out in the past indicates that the connection of ENSO with other climatic oscillations explains the diversity of effects on hydroclimatic variables, being the possible combinations of the phases of these oscillatory processes multiple and the resulting atmospheric state different for each one (Alexander et al., 2002; Zhang et al., 2018; Beltrán and Díaz, 2020).

One of the connections with the greatest influence on atmospheric dynamics over the North Atlantic, the Eastern Pacific, and much of the American continent is the one between ENSO and the North Atlantic Oscillation (NAO) (Whan and Zwiers, 2017; Zhang et al., 2018; Fereday et al., 2020). NAO is a pattern of atmospheric circulation caused by the movement of polar and subtropical air masses and is represented by the atmospheric pressure difference between the low of Iceland and the high of the Azores (Visbeck et al., 2001). The ENSO/NAO relationship depends on ocean-atmosphere interaction processes capable of connecting the conditions of the Pacific Ocean with those of the North Atlantic (Zhang et al., 2018). Different authors hypothesize wide mechanisms of this interaction. Recent studies suggest that the ENSO and NAO teleconnection consists of a relationship between the atmospheric circulation over North Atlantic and the anomalies in the Pacific, but the physical mechanism has not been fully addressed (Li and Lau, 2012). This link is associated with changes in the intensity of the northeast trade winds, stormy formations, and the displacement of the Intertropical Convergence Zone (ITCZ) over the Tropical Atlantic (Whan and Zwiers, 2017). To understand the ENSO/NAO teleconnection is essential to know the diversity of ENSO in its spatial structure and the possible mechanisms that explain the connection with the North Atlantic. Observations and simulations have detected so far that ENSO events can be classified into two categories, those focused especially on the Central Pacific (CP) and those most affected towards the Eastern Pacific (EP) (Ashok and Yamagata, 2009; Kao and Yu, 2009; Sullivan et al., 2016).

Additionally, it has been identified that EP and CP El Niño events tend to be accompanied by a negative phase of the NAO, and CP La Niña by a positive one. However, for EP La Niña events there is no clear tendency to infer which phase of the NAO is more frequent (Zhang et al., 2015, 2018). Therefore, there is not a single and stable link between ENSO and NAO in the cold phase of ENSO, giving this relationship a more complex character.

Previous studies have concluded that, for now, it is only possible to affirm that the ENSO/NAO connection tends to be linear when ENSO is classified as PC, while for EP events, the relationship appears to be non-linear (Zhang et al., 2015, 2018). These contrasts are attributed to non-linear ocean-atmosphere interactions over the Tropical Eastern Pacific. On the other hand, the response of the atmosphere on the CP to SST anomalies seems to be highly linear. The most recent studies suggest that this occurs because the center of action of the ocean-atmosphere relationship is within the Pacific's warm pool, an area characterized by having on average a higher SST (Dommenget et al., 2013; Capotondi et al., 2015). Therefore, a positive or negative anomaly quickly triggers atmospheric processes such as deep convection. On the contrary, the atmospheric response in EP to SST anomalies may be non-linear because the major relationship is located in an area with lower SST than the CP, along with a later response of the atmosphere. For example, if El Niño happens in this sector, only sufficiently positive SST anomalies could exceed the threshold for deep convection (Dommenget et al., 2013; Zhang et al., 2018).

The results show that despite its great internal variability, a negative anomaly in the NAO usually coincides with El Niño events, while a positive anomaly does not always correspond to a La Niña event (Zhang et al., 2015, 2018). Also, it was observed that the impact of ENSO on NAO is seasonally modulated; for example, anomalies observed during November-December are opposite to those in January-March (Moron and Gouirand, 2003). There are several theories to explain how the ENSO/NAO connection occurs: the first mechanism suggests that when an ENSO event reaches its maximum development during December-January-February (DJF), it can stimulate the Rossby waves that usually extend to the North Atlantic, modifying quasi-standing waves' structures. Interactions of the medium flow also strengthen these waves, influencing in this way the atmospheric circulation over the North Atlantic during the JFM period (Cassou and Terray, 2001; Alexander et al., 2002; Drouard et al., 2015).

Another proposed mechanism sustains that the connection occurs through the formation of synoptic eddies that cause an energy dispersal of synoptic waves traveling from the North Pacific to the North Atlantic, causing low-frequency atmospheric circulation anomalies (Li and Lau, 2012). Yet another hypothesis indicates that during El Niño events, energy transport is favored between the North Pacific and the North Atlantic at low latitudes. In contrast, during La Niña events, less intense propagation occurs at higher latitudes and therefore has a shorter range or influence over North America and the North Atlantic (Li and Lau 2012; Drouard et al. 2015). Recently, Zhang et al. (2018) proposed that there can be several mechanisms linking ENSO/NAO, and they vary depending on whether they are a CP or EP ENSO (Visbeck et al., 2001; Whan and Zwiers, 2017; Wang et al., 2018). To explore the teleconnection of ENSO and NAO, the linear correlation among the indices representing each oscillation was investigated, and composite anomaly maps were plotted to visualize the contrasts for different types of ENSO.

2. Metodology

2.1 Data

This study was conducted using the climatic index representing ENSO and NAO. Table I contains the description of each index selected to carry out the research. The SST data was taken from the ERSST V5 (Huang et al., 2017). The information on variables such as precipitation, wind, outgoing longwave radiation (ORL) and vorticity was taken from the NCEP/NCAR Reanalysis-1 with 2.5º × 2.5º spatial resolution and monthly time resolution (Kalnay et al., 1996). The analysis was carried out for the period 1981-2016 and the anomalies were calculated by taking the climatological mean between 1991 and 2020.

Linear correlation analyses were performed to evaluate the ENSO/NAO relationship using the indices presented in Table I. The climatic index from 1950 to 2016 was obtained from the National Oceanic and Atmospheric Administration (NOAA) Climate Prediction Center (CPC) and the NOAA Earth System Research Laboratory's Physical Sciences Division (PSD). Table I presents a short description of the indices selected. The December-January-February (DJF) seasonal series of the ENSO indices were related to the NAO index seasonal series for January-February-March (JFM). Those seasons were chosen considering that previous studies have shown that ENSO events reach their peak phase during DJF and that the largest impact on NAO can be found during JFM (e.g., Zhang et al., 2015).

2.2 Methods

All correlations were estimated for different combinations of years using Pearson correlation following the expression:

$$r = \frac{1}{n-1}\sum_{i=1}^{n}\left(\frac{x_i-\bar{x}}{\sigma_x}\right)\left(\frac{y_i-\bar{y}}{\sigma_y}\right) = \frac{\sigma_{xy}}{\sigma_x\sigma_y} \tag{1}$$

where σ_{xy} is the covariance between variables X and Y, and σ_x and σ_y are the variance. The Pearson correlation coefficient varies between –1 and 1, where an absolute value of 1 indicates that the variables present a perfect linear relationship, where they can be directly (positively) or inversely (negatively) related. A correlation coefficient of 0 indicates no linear relationship between the two variables (Gutiérrez et al., 2004).

To establish whether the correlation is significant, a hypothesis test was performed where *Ho* means that the correlation is not significantly different from 0, and *Ha* implies that the correlation is significantly different from 0. For this purpose, a two-tailed t-test was performed, where t and P values were taken. Statistically significant values were obtained at 95% when $|t| > t^*$, where t^* represents the critical

Table I. Indices used to represent ENSO and NAO.

Index	Description
Niño1+2	Extreme Eastern Tropical Pacific SST (0-10º S, 90º-80º W). Data from the CPC.
Niño 3	Eastern Tropical Pacific SST (5º N-5º S, 150º-90º W). Data from the CPC.
Niño 3.4	East Central Tropical Pacific SST (5º N-5º S) (170º-120º W). Data from the CPC.
Niño 4	Central Tropical Pacific SST (5º N-5º S, 160º E-150º W). Data from the CPC.
ONI	Oceanic El Niño Index calculated as the three-month running mean of SST anomalies in the Niño 3.4 region. The climatology used for the anomaly was form 1986 to 2015. Data from the CPC.
SOI	Southern Oscillation Index calculated as the pressure difference between Tahiti and Darwin. Data from the CPC.
BEST	Bivariate ENSO timeseries calculated from combining a standardized SOI and a standardized Niño 3.4 SST time series. The values are averaged for each month and then, a three-month running mean is applied to both time series. Data from PSD.
MEI	Multivariate ENSO Index Version 2. MEI is the time series of the leading combined Empirical Orthogonal Function (EOF) of five different variables (sea level pressure [SLP, sea surface temperature [SST], zonal and meridional components of the surface wind, and outgoing longwave radiation [OLR]) over the tropical Pacific basin (30º S-30º N and 100º E-70º W). Data from the PSD.
TNI	The Trans-Niño Index is calculated as standardized Niño 1+2 minus the Niño 4 with a five-month running mean applied, which is then standardized using the 1950-1979 period. Data from the HadISST 1.1 dataset.
NAO	The normalized pressure difference between a station in the Azores and one in Iceland (Jones et al., 1997).

CPC: National Oceanic and Atmospheric Administration Climate Prediction Center; PSD: NOAA Earth System Research Laboratory's Physical Sciences Division; HadISST: Hadley Centre Global Sea Ice and Sea Surface Temperature.

value for a given n. (Krzywinski and Altman, 2013). Table II presents the ENSO years' classification according to their dominant longitudinal position. For the ENSO event classification, we followed previous studies (Kim et al., 2009; Zhang et al., 2015, 2018) where they were classified into CP if the maximum anomaly occurred west of 150º W, and EP when the anomaly occurred east of this latitude for the period September-February, when ENSO is in its developing and mature phases. The events influenced by the eruptions of El Chichón (1982-1983) and Pinatubo (1991-1992) volcanoes, and the ENSO events whose anomalies cover both CP and EP regions, were discarded for the correlation analysis. Table III presents the designed cases, including the events and sample size for each one. In addition to the linear correlation for different sets of years, composite maps were produced with the anomalies of the SST, wind, surface precipitation rate, and ORL variables.

3. Results and discussion

The correlation coefficients between seasonal time series are presented in Table IV (bold numbers are statistically significant at a confidence level of 95%). Furthermore, the signs of R correspond to an inversely proportional ENSO/NAO relationship; that is, an El Niño event tends to be accompanied by a negative phase of NAO, and La Niña for a positive phase. As suggested in previous studies, the results show a difference in the relation's direction when the ENSO is located in the EP or the CP (Zhang et al., 2015, 2018).

R values for case 1, considering every year, ranged from –0.02 to 0.14 (t | > 1.99, P < 0.05), and were not significant at 95%, which suggests no linear relationships between the NAO index and ENSO. For Case 2, where the years with volcanic eruptions were removed, t R values continued to be close to 0, varying between –0.9 and 0.10 (t | > 2.00, P < 0.05).

Table II. Classification of ENSO years according to their longitudinal position, years with mixed events, and years with volcanic eruptions*. Classification according to Zhang et al. (2018).

	El Niño	La Niña
Eastern Pacific (EP) (9, 8)	1951/52, 1952/53, 1963/64, 1965/66, 1969/70, 1972/73, 1976/77, 1997/98, 2015/16	1954/55, 1955/56, 1664/65, 1967/68, 1971/72, 1984/85, 1995/96, 2005/06
Central Pacific (CP) (9, 8)	1953/54, 1957/58, 1968/69, 1977/78, 1979/80, 1986/87, 2002/03, 2004/05, 2009/10	1973/74, 1974/75, 1975/76, 1988/89, 1998/99, 2000/01, 2010/11, 2011/12
Mixed events	1987/88, 2006/07	1970/1971, 1999/00, 2007/08
Volcanic eruptions	(1) 1982, 1983, 1984 (2) 1991, 1992, 1993, 1994	

*Classification according to Zhang et al. (2018).
Volcanic eruptions: (1) and (2) represent the years of influence of El Chichón and Pinatubo eruptions, respectively.

Table III. Correlation cases.

Case	1	2	3	4	5	6	7	8	9
N	67	60	22	52	38	28	27	19	17
Years	All	All, except volcano years	All, except volcano and ENSO years	All, except volcano and EP La Niña years	ENSO years	El Niño and CP La Niña years	La Niña and EP El Niño years	EP El Niño, EP La Niña years	CP El Niño and CP La Niña years

Table IV. Linear correlation coefficients between DJF-ENSO and JFM-NAO indices. Bold values are two-tailed t-test significant values (*t*-statistic and *P* value).

Case	n	Niño 1+2	Niño 3	Niño 3.4	Niño 4	ONI	SOI	BEST	MEI	TNI
1	67	0.14	0.05	0.01	–0.02	–0.02	–0.01	–0.01	0.07	0.08
2	60	0.08	–0.03	–0.07	–0.08	–0.08	0.09	–0.09	–0.02	0.10
3	22	0.13	0.10	0.20	0.29	0.17	–0.26	0.23	0.22	–0.30
4	52	–0.03	–0.18	–0.22	–0.21	–0.24	0.16	–0.19	–0.16	0.19
5	38	0.17	–0.02	–0.13	–0.25	–0.13	0.19	–0.16	–0.06	**0.33***
6	28	0.01	–0.26	**–0.39***	**–0.50***	**–0.41***	0.24	–0.34	–0.31	**0.55***
7	27	0.26	0.10	–0.01	–0.13	0.01	0.11	–0.05	–0.04	**0.40***
8	17	**0.67***	**0.71***	**0.75***	**0.75***	**0.76***	**–0.72***	**0.74***	**0.76***	–0.10
9	17	–0.45	**–0.68***	**–0.71***	**–0.74**	**–0.72***	**0.58***	**–0.63***	**–0.64***	**0.68***

Bold numbers are two-tailed t-test significant values (t-statistic and P value) statistically significant at a 95% confidence level.

These results did not represent a significant change compared to those of the previous case. Regarding Case 3, made up of neutral years, the results were similar, with R values between –0.30 and 0.29 ($t \,|> 2.08$, $P < 0.05$). R values increased for Case 4 excluding the years with eruptions and EP La Niña, ranging between –0.24 and 0.19 ($t \,|> 2.08$, $P < 0.05$), but they are not significantly different of 0. In Case 5, which only considered the years with ENSO events, R ranged between –0.25 and 0.33 ($t \,|> 2.02$, $P <$ 0.05), showing significant correlation values only for the TNI index. The results of the first five cases are consistent with previous studies that did not find a significant connection between ENSO and NAO (Wang, 2002).

Case 6, which considers only the years of El Niño and CP La Niña, showed a clear increment of R values, varying between –0.50 and 0.55 ($t \,|> 2.08$, $P <$ 0.025), and a significant correlation with the TNI index, which measures the SST gradient in the Eastern Pacific, as well as with the ONI, Niño 4 and Niño 3.4 indices, which measure the SST of the central Pacific. The results obtained for this case allowed to consider the hypothesis of the non-linearity effect provided by the data from the years with EP La Niña events, and the linearity of CP ENSO. R coefficients increased by up to 0.4 with respect to the former cases. As suggested previously (and shown in Figure 1) the lack of linearity of the relationship may occur due to a different and more sensitive NAO response to the location of La Niña anomalies (Zhang et al., 2015, 2018) that can be reflected in differential impacts in oceanographic and atmospheric variables. For Case 7, considering only years of La Niña and EP El Niño, R decreased ranging between –0.13 and 0.40 ($t \,|> 2.08$, $P < 0.025$), with only a TNI result of 0.40. Case 8 for ENSO EP events showed R coefficients between –0.10 and 0.76 ($t \,|> 2.12$, $P < 0.05$). This change of signs suggests that the direction of the relationship between NAO and events in EP is opposite to that of the events classified as CP. Finally, for Case 9, which includes only CP events, R showed high values varying between –0.74 and 0.68 ($t \,|> 2.12$, $P < 0.05$). This last scenario is more restrictive than Case 6 because it omits EP El Niño records, which explains why this case shows the highest R coefficients and can indicate the importance of separating both ENSO types of events when it is needed to evaluate their impacts.

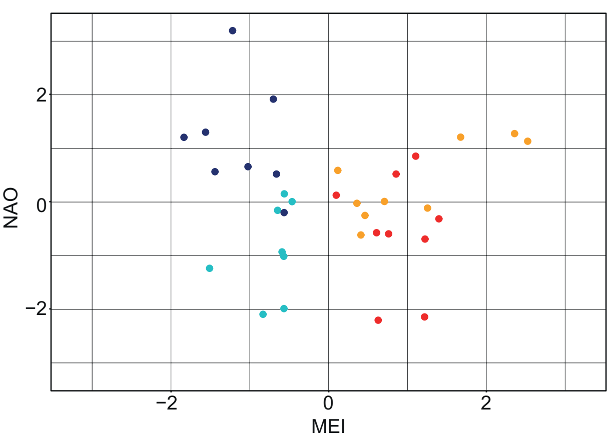

Fig. 1. Scatterplot of the MEI and NAO indices during DJF and JFM, respectively. Dark blue: CP La Niña; light blue: EP La Niña; red: CP El Niño; orange: EP El Niño.

The NAO/El Niño 1+2 relationship showed the highest R coefficient in Case 8, but in the rest of the cases its values are low, suggesting that the dynamics of the SST of this Pacific region do not have a clear linear link with the NAO behavior. Results for El Niño 3 are similar to those obtained for El Niño 1+2, with the exceptions of cases 8 and 9, which have an R coefficient of 0.71 and –0.68, while for the rest the values are low, showing a possible highest linear relation with westward SST anomalies. For all the other indices, that is, El Niño 3.4, El Niño 4, ONI, SOI, BEST, MEI and TNI, results are similar among them. The highest R coefficients for each relationship are reported for cases 6, 8 and 9. Furthermore, all coefficients have an inversely proportional ENSO/NAO relationship, whose linear link can be better appreciated when La Niña EP events are not included and are opposite when EP or CP centered anomalies are considered.

The results presented in Table IV show that considering each year in the correlation does not reveal any significant link between ENSO and NAO, which is why until recently this dependency was unnoticed and even ruled out. The R coefficients obtained for Case 6, which are higher than the others, are those that support the nonlinearity hypothesis of the ENSO/NAO relationship. That is, the response of the atmosphere over the Pacific to an EP La Niña event does not have a single or determined influence on atmospheric dynamics over the North Atlantic, which suggests firstly that circulation changes over the Pacific can influence modifications in the atmospheric circulation over North Atlantic (Graf and Zanchettin, 2012) and secondly that their influence is modulated by the position of ENSO anomalies on the equatorial Pacific (Cai et al., 2020). Of all the indices considered, the TNI/NAO relationship showed the highest R coefficients. TNI is calculated to represent the Pacific SST gradient, therefore it contains information about the SST variation from the Niño 1+2 region to the El Niño 4 in a single index. Thus, its variation manages to better reveal the connection between the Pacific and the North Atlantic via ENSO events.

The composite maps in Figures 2 to 9 depict the difference between the anomalies caused by a CP or EP ENSO event in SST, vector wind, surface precipitation rate, ORL, and vorticity variables over the Pacific and Atlantic oceans. Figure 2 contains the composite SST (ºC) anomalies for the CP and EP La Niña. During CP La Niña years, the greatest negative anomalies are concentrated in the Equatorial Pacific, ranging from –1.5 to –0.5 ºC, being more intense between 180º and 160º W. Negative anomalies are also present throughout the western coast of America, particularly in the California coast. Over the Atlantic, negative anomalies are located around 20º N with values between –0.5 and 0 ºC. The positive SST anomalies are evident in the North Pacific with values between 0.5 and 1.3 ºC around 160º W and in the South Pacific waters.

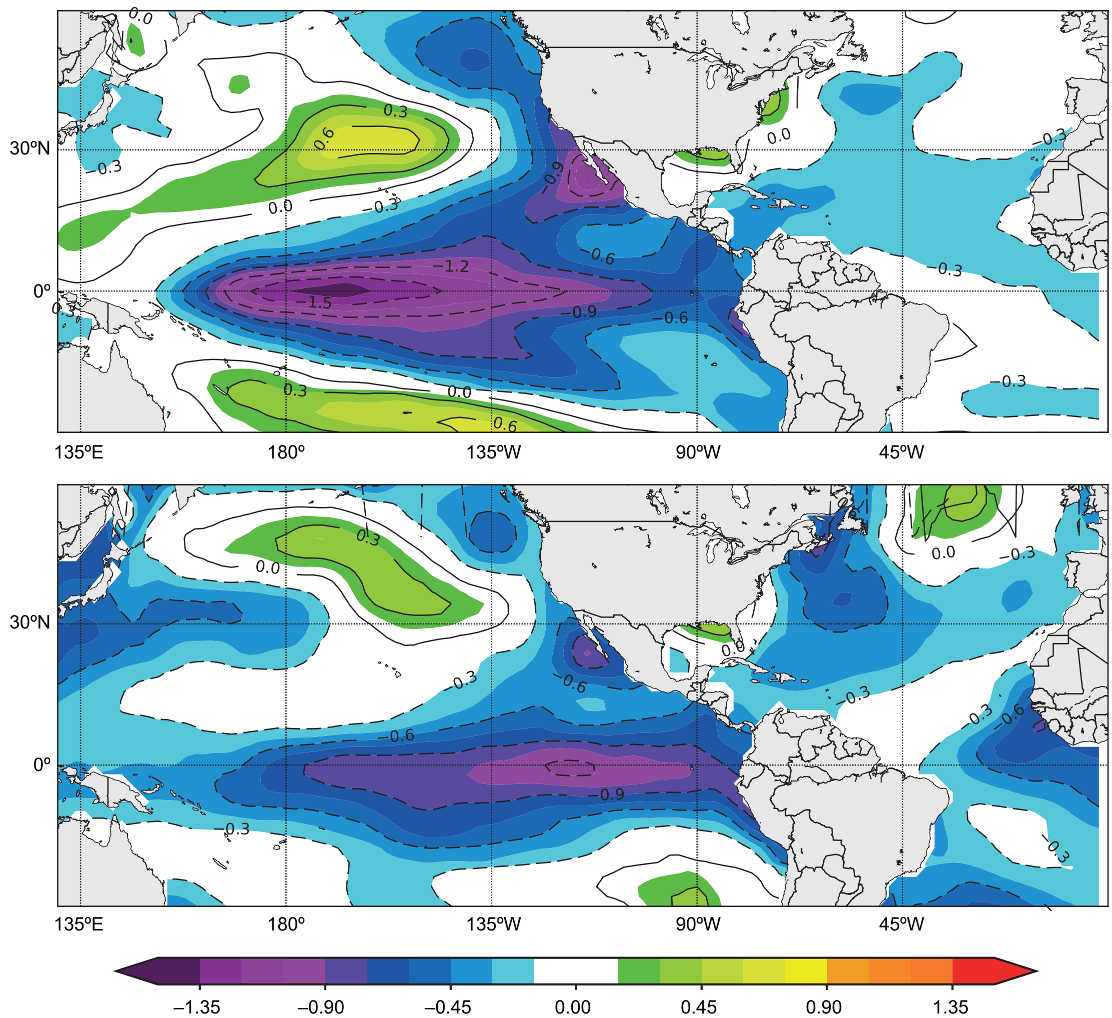

Fig. 2. Composite SST (ºC) anomalies for CP La Niña (top) and EP La Niña (bottom). Data source: ERSST NOAA V5 Climatology: 1991-2020.

During EP La Niña, negative anomalies also occur with SST lower values nearby 120º W, ranging from –1.25 to –0.25 ºC along the Equatorial Pacific but in a smaller area between 180 and 80º W. The anomalies on the coasts of South America are less notable than in the previous case. On the contrary, on the North Atlantic they cover a larger area and reach lower values. The maximum positive anomalies are present in a smaller area of the North Pacific limited to a region between 150 and 180º W, whilst in the south they appear only in a sector off the coast of Chile and Peru.

The composite SST (ºC) anomalies for CP and EP El Niño events (Fig. 3) show the evident differential maximum in temperature throughout the Equatorial Pacific. During CP El Niño, the average positive anomalies ranged between 0.1 and 1.5 ºC and from 180 to 80º W, with maximum values around 160º W. In addition, an increase in temperature is observed along the west coast of the United States, the Antillean arc in the Caribbean and northern Japan. In the latter, anomalies exceeded 1.5 ºC. In contrast, the only negative anomalies with values between –0.25 and –0.75 ºC are found in the North Atlantic, East China Sea, Gulf of Mexico, Indonesia, and east of the South Pacific. These SST anomaly patterns associated with ENSO events show that that, in effect, they are well separated, validating the classification.

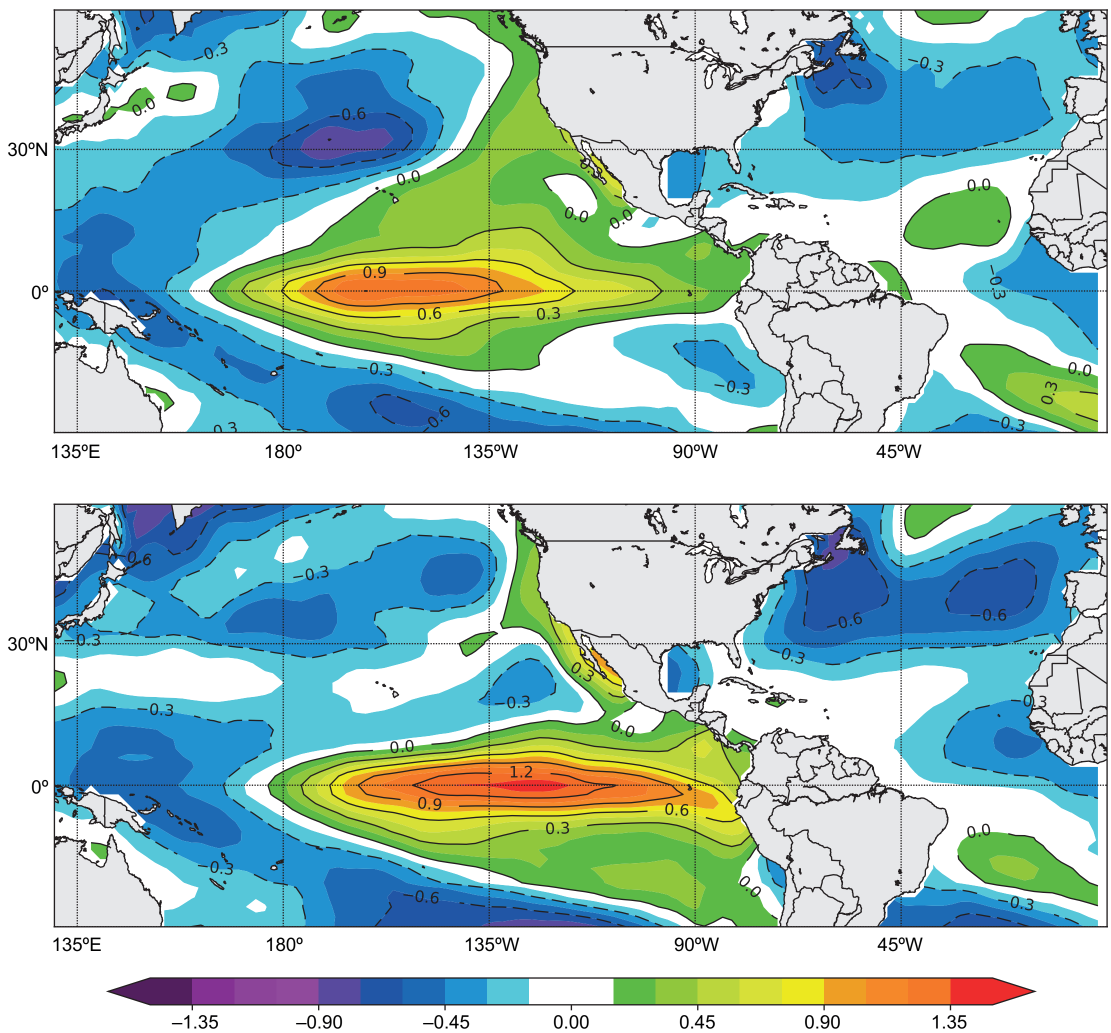

Fig. 3. Composite SST (ºC) anomalies for CP El Niño (top) and EP El Niño (bottom). Data source: ERSST NOAA V5 Climatology: 1991-2020.

As shown in previous studies, the amplitude of CP La Niña anomaly is larger than EP La Niña, and the opposite for El Niño events (Ashok et al., 2007; Kao and Yu, 2009; Kug et al., 2009; Zhang et al., 2015).

The composite vector wind anomalies for CP and EP La Niña are shown in Figure 4. During La Niña years, northward wind anomalies were found in both events. For CP La Niña the maximum anomalies are located around 180º W with increases around 3 m s^{-1}. Additionally, in the northeast Pacific, a westward and southward anomaly was found in the west of the USA. The largest anomalies for EP La Niña are located in Central-North Pacific between 30º and 40º N with values ranging from 2.7 to 1.2 m s^{-1}. Regarding the Equatorial Pacific, EP La Niña anomalies have low intensity; the highest values were found to be around 1.8 m s^{-1}, located between 160º and 140º N. As for the North Atlantic, the highest anomalies were found for EP La Niña, with an eastward anomaly of 2 m s^{-1} around 30º N. As shown previously, the anomalies between both types of La Niña in the North Atlantic tend to be in opposite direction (Zhang et al., 2015).

Figure 5 depicts the composite vector wind anomalies for CP and EP El Niño. In this case, greater differences are observed. In this scenario there are eastward anomalies with an increase of 2.4 m s^{-1} around 180º W in the northeast Pacific, with eastward

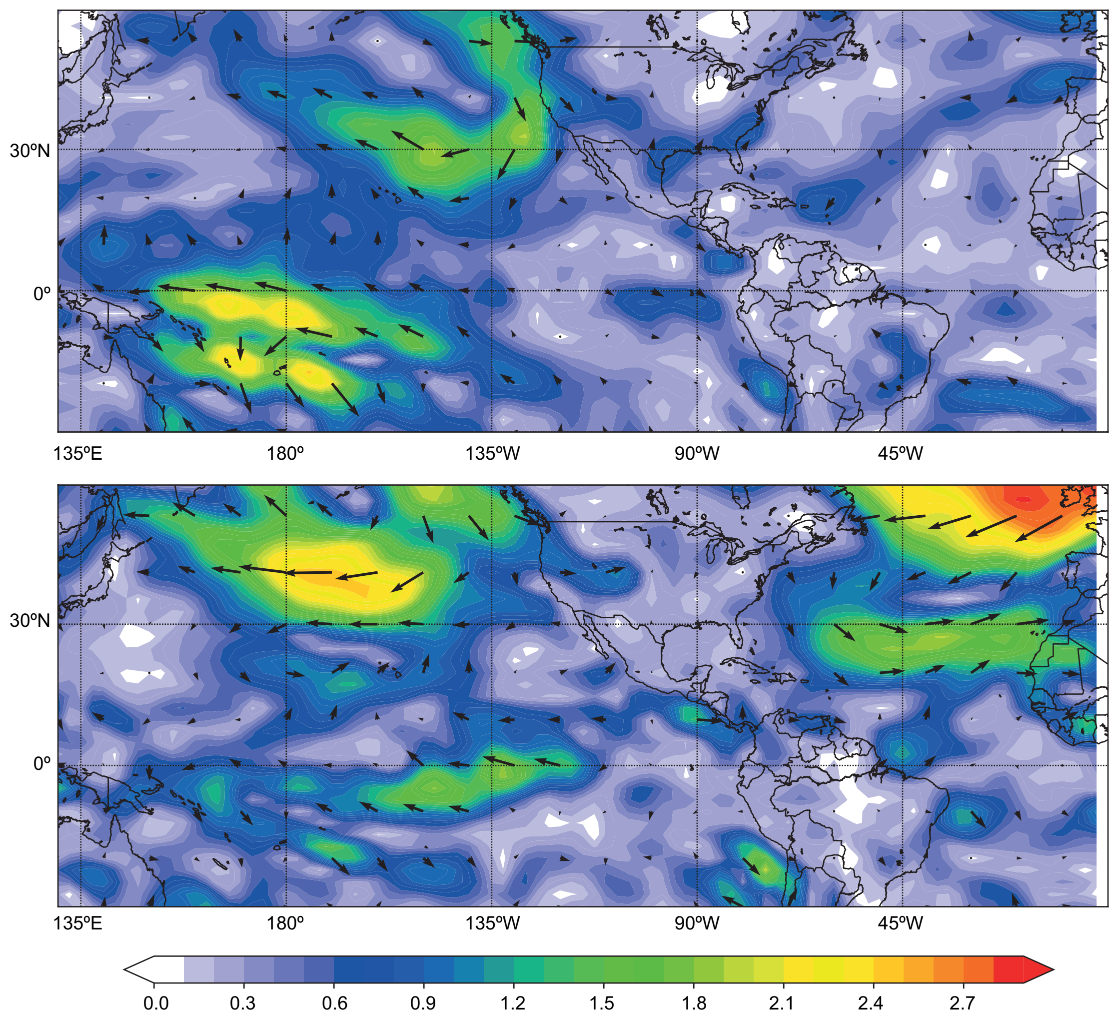

Fig. 4. Composite 1000 mb vector wind (m s^{-1}) anomalies for CP La Niña (top) and EP La Niña (bottom). Data source: NCEP/NCAR Reanalysis-1 Climatology: 1991-2020.

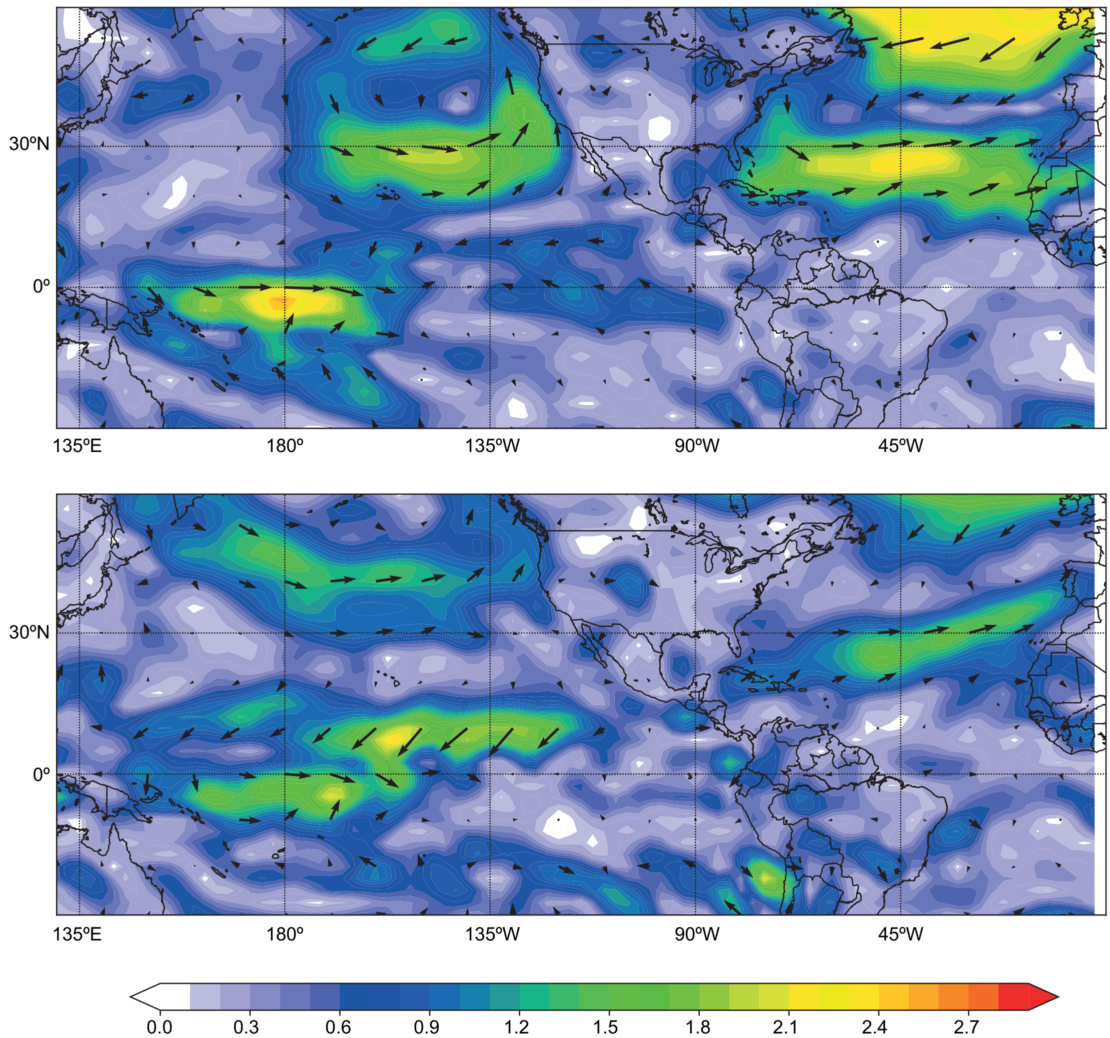

Fig. 5. Composite zonal wind (m s^{-1}) anomalies for CP El Niño (top) and EP El Niño (bottom). Data source: NCEP/NCAR Reanalysis-1 Climatology: 1991-2020.

anomalies near 2 m s^{-1} at 30º N and 140º W. For this event, eastward wind anomalies are shown in the North Atlantic at 30º N and westward at 50º N, with magnitudes 2 and 2.4 m s^{-1}, respectively. For EP El Niño, the greatest anomalies are located northward around 160º W in the Equatorial Pacific, and extend between 180º and 120º W. The north Pacific showed 2 m s^{-1} eastward anomalies near 40º N, between 160º E and 120º W. In the North Atlantic, the wind eastward anomalies are lowest, with greatest values around 1.4 m s^{-1}.

Figure 6 shows composite anomalies of the surface precipitation rate for CP and EP La Niña. During CP La Niña years, the anomalies are located around 150º E and 120º W at the Equatorial Pacific, with greatest values (4 mm d^{-1}) in 170º W. Smaller areas located on the west coast of the United States, the Gulf of Mexico, and small sectors on the Atlantic also show reductions in the surface precipitation rate. The positive anomalies stand out in the western Pacific in Indonesia, extending into the North and South Pacific surrounding the Equatorial Pacific zone. The maximum negative anomalies are located in the north of the South Pacific near 170º E with values ranging from –4 to –1 mm d^{-1}. In addition, there is increased precipitation throughout the eastern coast of South America, the southern Caribbean Sea, the Amazon, and the Andes. The largest positive anomalies are

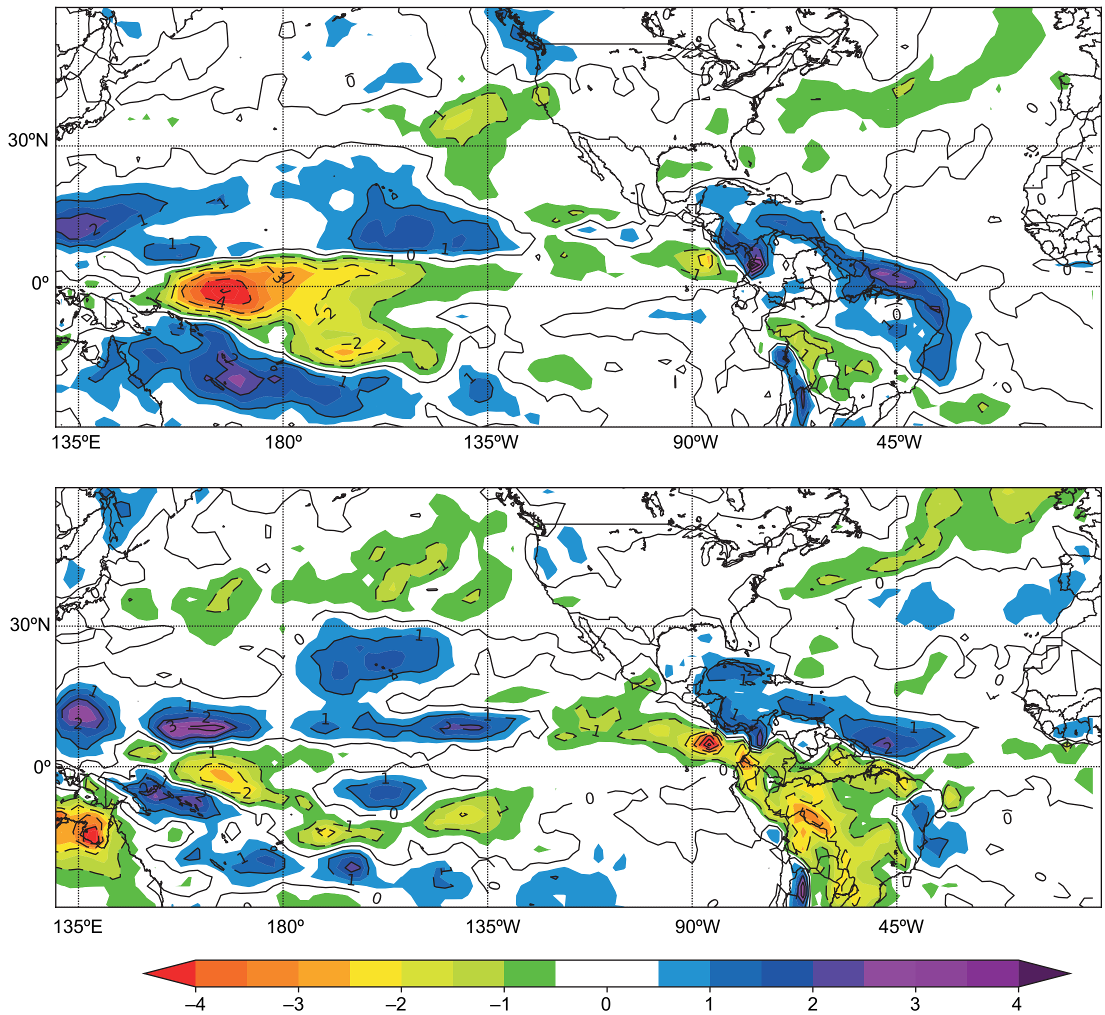

Fig. 6. Surface precipitation rate (mm day^{-1}) anomalies for CP La Niña (top) and EP La Niña (bottom). Data source: NCEP/NCAR Reanalysis-1 Climatology: 1991-2020.

concentrated in the maritime and continental zone of the Colombian Pacific, with an increase around 7 mm d^{-1}.

During EP La Niña years, the number of areas with negative precipitation anomalies increases, which includes northern Australia, the Equatorial Pacific around 170º E, extending slightly to the southeast, and the south of the Equatorial Pacific between 150º and 120º W. A large reduction zone of precipitation is located on the northeast of the Equatorial Pacific, with anomalies of up to –4 mm d^{-1} between 90º and 80º W. Precipitation anomalies in South America extend from the southern region of Colombia, Ecuador, Peru and the Amazon. Regarding the tropical Pacific, there is no central region where the maximum precipitation anomalies are observed as in CP El Niño. The positive anomalies for this case are present in the south of the Philippine Sea and north Australia. In addition, there is another significant anomaly zone that begins in the continental zone of the Colombian Pacific, the entire Caribbean Sea and south of the North Atlantic with anomalies of up to 2 mm d^{-1}. Other areas where surface precipitation rates increase are located in the north of Japan, the south of the North Pacific and the North Atlantic.

Figure 7 shows composite anomalies of surface precipitation rates for CP and EP El Niño. During CP El Niño events, the positive anomalies are located throughout the Equatorial Pacific. The highest

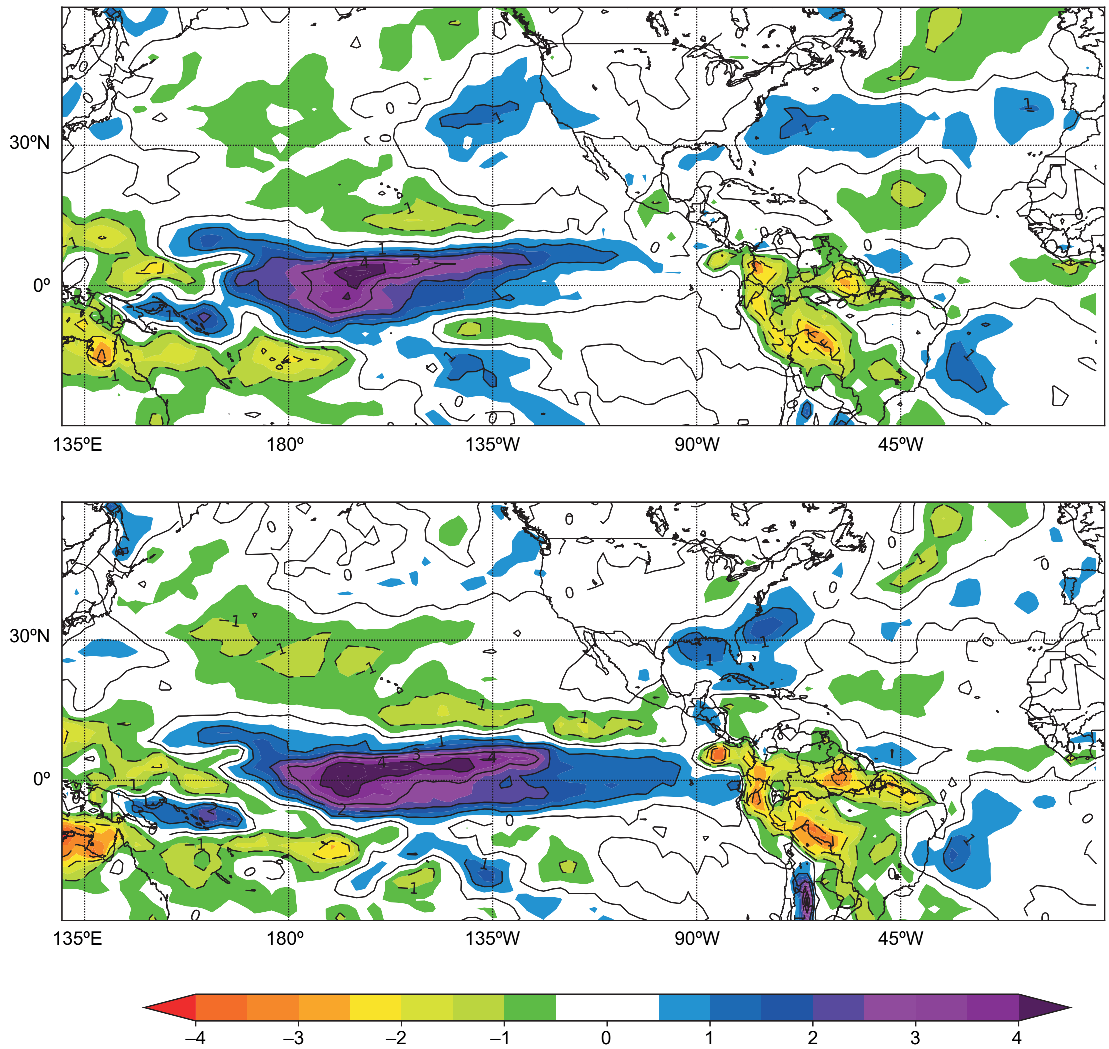

Fig. 7. Surface precipitation rate (mm day^{-1}) anomalies for CP El Niño (top) and EP El Niño (bottom). Data source: NCEP/NCAR Reanalysis-1 Climatology: 1991-2020.

positive anomalies are concentrated around 165º W, with magnitudes greater than 4 mm d^{-1}. Additionally, CP El Niño presents positive anomalies in the North Atlantic from the east coast of the United States to near the coast of Portugal. Another positive anomaly zone is located on the west coast of the United States and in the southwestern Atlantic zone in eastern Brazil, with magnitudes of up to 1.5 mm d^{-1}. Positive anomalies are located in the Western Pacific off the northeast coast of Australia and the Coral Sea, in addition to the south of the East China Sea, with anomalies down to –3 mm d^{-1}. There are negative anomalies in a large part of the northern territory of South America, mainly in the Colombian Pacific coast, reaching as far as Costa Rica and extending south through Ecuador, Peru and Bolivia, and to Northern Brazil towards the Equatorial Atlantic. The maximum anomalies in South America are located on the Colombian Pacific coast with records up to –3 mm d^{-1}.

The results are consistent with previous studies that show different patterns and influence over the precipitation anomalies when two types of ENSO are considered due the divergent atmospheric anomalies caused by each type of event. For example, it is clear that in South America precipitation anomalies during a cold ENSO phase have stronger and more extensive effects in the CP event than EP, and the opposite occurs during El Niño (Tedeschi et al., 2015).

During EP El Niño there are positive precipitation anomalies throughout the Equatorial Pacific, except for northern Indonesia, where they are negative. The highest anomalies are around 165º W with increased surface precipitation rates throughout the tropical Pacific. In addition, there are increases of up to 4 mm d^{-1} from Chile (along the Andes) to southern Peru. On the other hand, the east coast of the United States and the north of the Gulf of Mexico show increases of up to 2 mm d^{-1}. The negatives anomalies in EP El Niño events are quite pronounced in the northwest of Australia, with a decrease of around 4 mm d^{-1}; alongside, there are negative anomalies in the north and south of the Equatorial Pacific. Negative anomalies of around –2 mm d^{-1} occur in the American continent starting from the south of Central America (Costa Rica and Panama) to the south and east of Colombia, Ecuador, Peru, the Amazon territory, Brazil, Uruguay, and Paraguay.

Figure 8 displays the ORL for CP and EP La Niña, which shows important differences. For CP La Niña in the Equatorial Pacific, the greatest positive anomalies (25 W m^{-2}) are located around 170º E, with values greater than 5 W m^{-2} between 160º E and 140º W. In the other hand, around 30º N there are

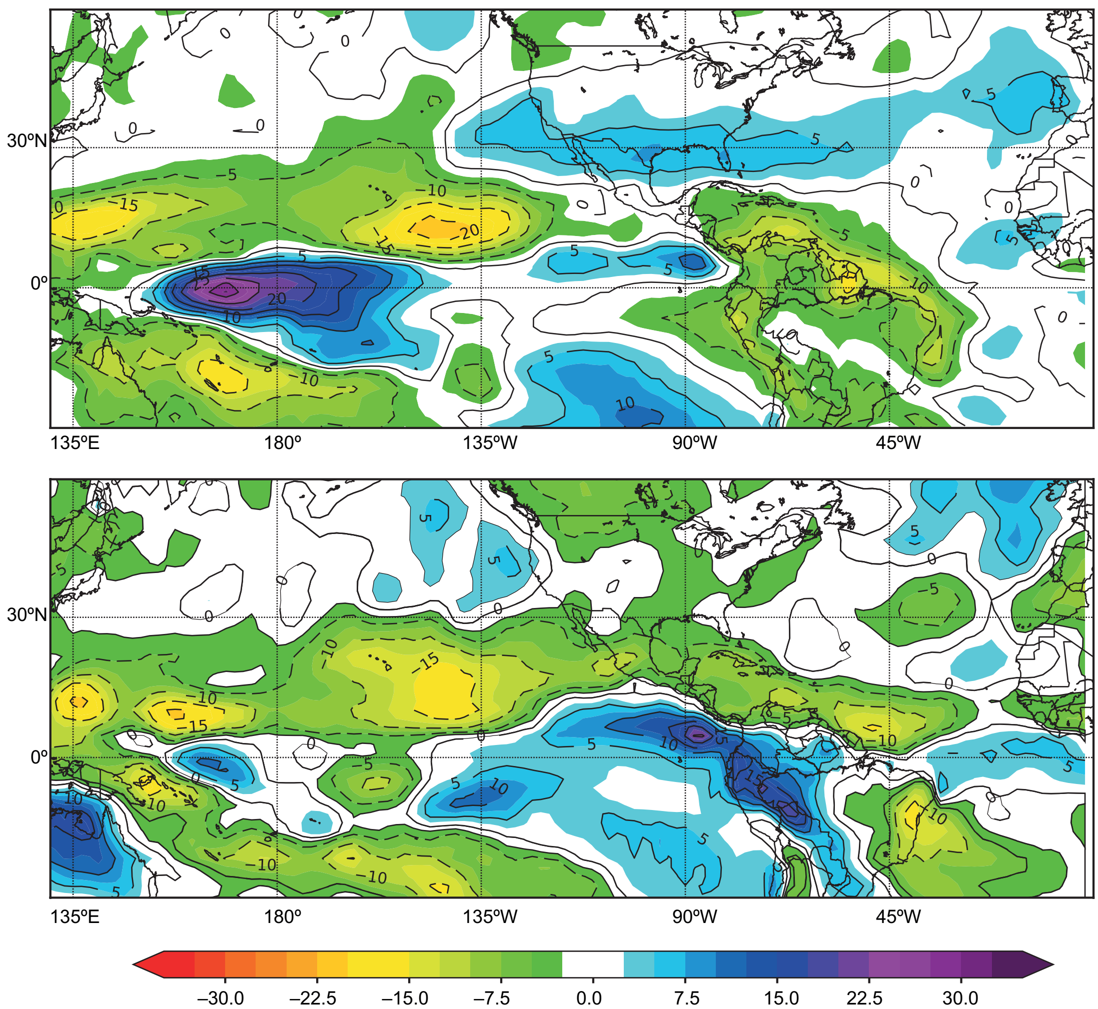

Fig. 8. Composite ORL (Wm^{-2}) anomalies for CP La Niña (top) and EP La Niña (bottom). Data source: NCEP/NCAR Reanalysis-1 Climatology: 1991-2020.

positive anomalies starting at 140º W and extending throughout North America to the North Atlantic up to 20º W. The greatest negative anomalies are shown in the north Equatorial Pacific around 140 ºW with values decreasing to -25 W m^{-2}. Additionally, positive anomalies extend from the equatorial Indopacific eastward to the tropics around the positive anomalies located in the Equatorial Pacific. Negative anomalies can be seen all over South America with greatest values in the coast of Peru, northeastern Brazil, and eastern Bolivia.

On the other hand, positive ORL anomalies for EP La Niña are located mainly in north Australia, south Equatorial Pacific between 140º and 120º W, and northwest South America, extending throughout the east Equatorial Pacific. Additionally, the Equatorial Atlantic also showed these positive anomalies. The equatorial and north Indopacific show negative ORL anomalies which extend eastward to the north and south hemispheres, with highest values around 10º N at 140º, 160º, and 140º W. The north Equatorial Atlantic, Caribbean and Gulf of Mexico show negative anomalies and which extend to the southern North Atlantic.

Additionally, the positive ORL anomalies for EP La Niña are located mainly in north Australia, the south Equatorial Pacific between 140º and 120º W, and northwest South America, extending throughout the eastern Equatorial Pacific and the Atlantic. The equatorial and north Indopacific showed negative ORL anomalies which extend eastward towards the northern and southern hemispheres, with highest values around 10º N at 140º, 160º, and 140º W. The north Equatorial Atlantic, Caribbean and Gulf Mexico show negative anomalies, which extend toward the southern North Atlantic.

Similar patterns of ORL anomalies for CP and EP El Niño are shown in Figure 9. The negative anomalies extend throughout the tropical Pacific, western Central America and the North Atlantic. Additionally, positive anomalies are located in northern South America, northern Australia and the south and north tropical Pacific. The main difference is in the anomaly magnitude, with maximum negative anomalies in the Pacific (-35 W m^{-2}) around 165º W and less than -5 W m^{-2} in the North Atlantic.

The comparison of composite maps shows that anomalies vary not only depending on whether the ENSO phase is warm or cold but also on whether it is concentrated in the central or eastern Pacific. In the Pacific, one of the most important aspects of ENSO impacts is deep convection, which highly depends on the total SST (climatological SST + SST anomalies) (Ashok and Yamagata, 2009; Dommenget et al., 2013). It is possible that the region presenting high total SSTs may trigger a fast-deep convection atmospheric response. Since this response is slow in the EP, it may not reach the convective threshold necessary to generate deep convection, so SST anomalies in this region will not always trigger an atmospheric dynamic response (Zhang et al., 2018), especially for cold events. As depicted in Figure 1, the similarity between the two types of El Niño in the ENSO-NAO teleconnection could potentially be attributed to the fact that the larger SST anomalies associated with EP El Niño might lead to a comparable atmospheric response for both events, although the CP region has a higher likelihood of triggering a convective response. In contrast, this similarity may not be observed in the case of La Niña. ORL anomalies are an indicator of deep convection and have an influence on precipitation and other atmospheric variables (Capotondi et al., 2021). Ss shown on our results, ORL anomalies have highest values in El Niño and CP La Niña, and lower values in EP La Niña, validating our hypothesis.

Based on the description of the composite maps obtained, we discuss below how the behavior of the anomalies in each scenario brings elements to propose different dynamic mechanisms that favor or attenuate the ENSO/NAO relationship in the established scenarios.

The maps in Figures 2 and 3 show the zonal gradients of the SST anomalies configured in each scenario. In the EP events, SST variations throughout the Tropical Pacific are less than in the CP cases. This feature can be associated with the mechanism based on the consideration that although freely propagating Rossby waves are only weakly excited in the atmosphere, zonal heating variations can give rise to forced Rossby stationary modes that influence atmospheric circulation on a planetary scale.

So, when the events reach the eastern sector and the zonal changes of SST are more homogeneous throughout the tropical belt, the forcing of the Rossby waves will be lower. The opposite will occur for CP

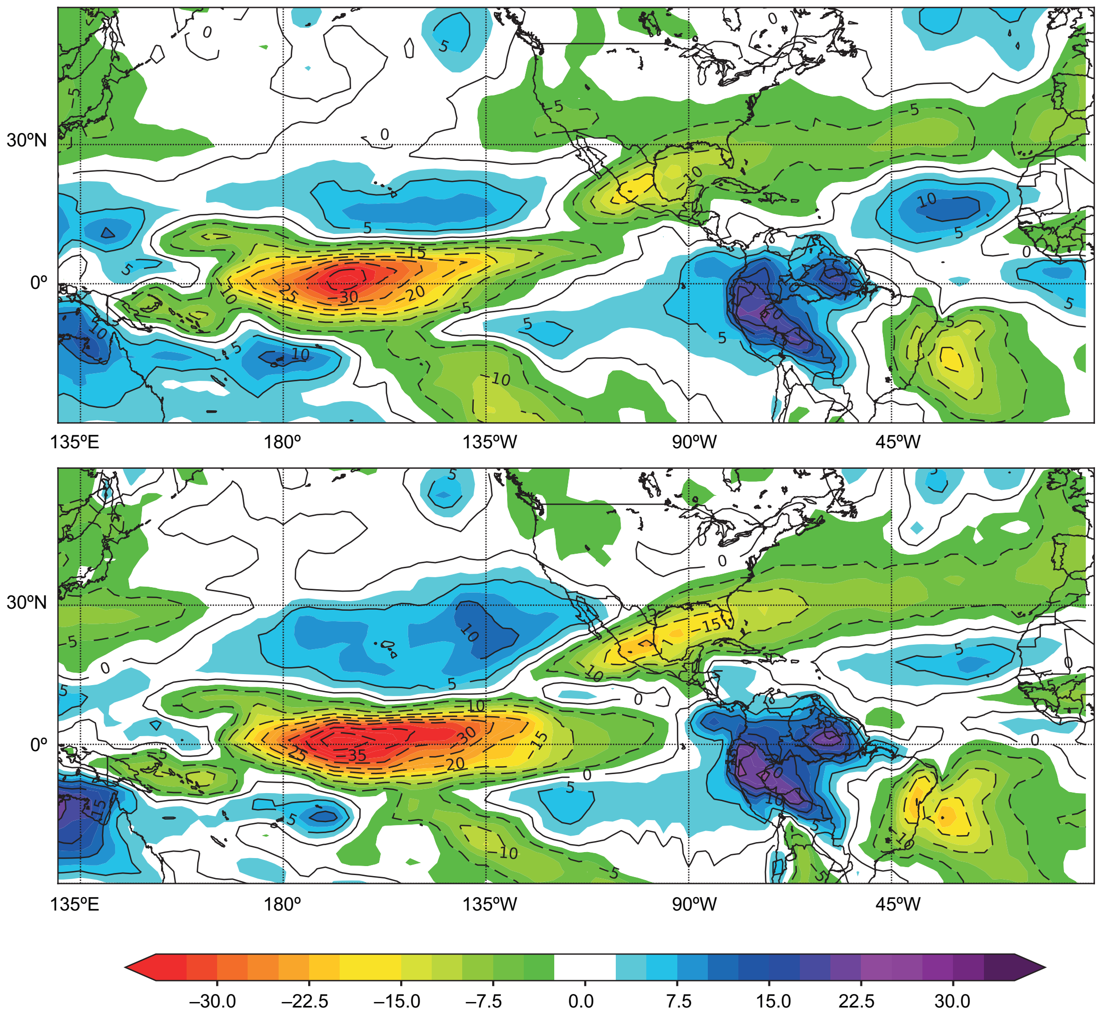

Fig. 9. Composite ORL (Wm^{-2}) anomalies for CP El Niño (top) and EP El Niño (bottom). Data source: NCEP/NCAR Reanalysis-1 Climatology: 1991-2020.

events when there is a greater SST zonal contrast between the central and eastern sectors. By having a lower forcing of the waves, the transport of momentum and energy that connects the dynamics of both basins also decreases.

Additional maps of vorticity anomalies for the 0.221 sigma level included in Figures 10 and 11 were created to complement this analysis. They also show a continuous band of anomalies that extends from the Tropical Pacific to the North Atlantic, crossing the North American continent. But for EP La Niña scenario, the strip presents a clear discontinuity on the continental sector, favoring the hypothesis of a weaker atmospheric connection, especially in this case.

Another aspect to highlight in Figures 2 and 3 is the difference between SST anomalies in the Atlantic. For El Niño scenarios, the area that presents changes is smaller, which can be related to another of the mechanisms proposed to understand the ENSO/NAO dependency. Some authors have suggested that when an ENSO process evolves, the SST of the tropical North Atlantic also presents atypical changes and that these SST anomalies, which continue to propagate towards the North Atlantic, are the ones affecting the atmospheric circulation of this region (Wu and He, 2019); however, in the maps for El Niño scenarios it is evident that the fluctuations in the tropical Atlantic are close to zero in large part of

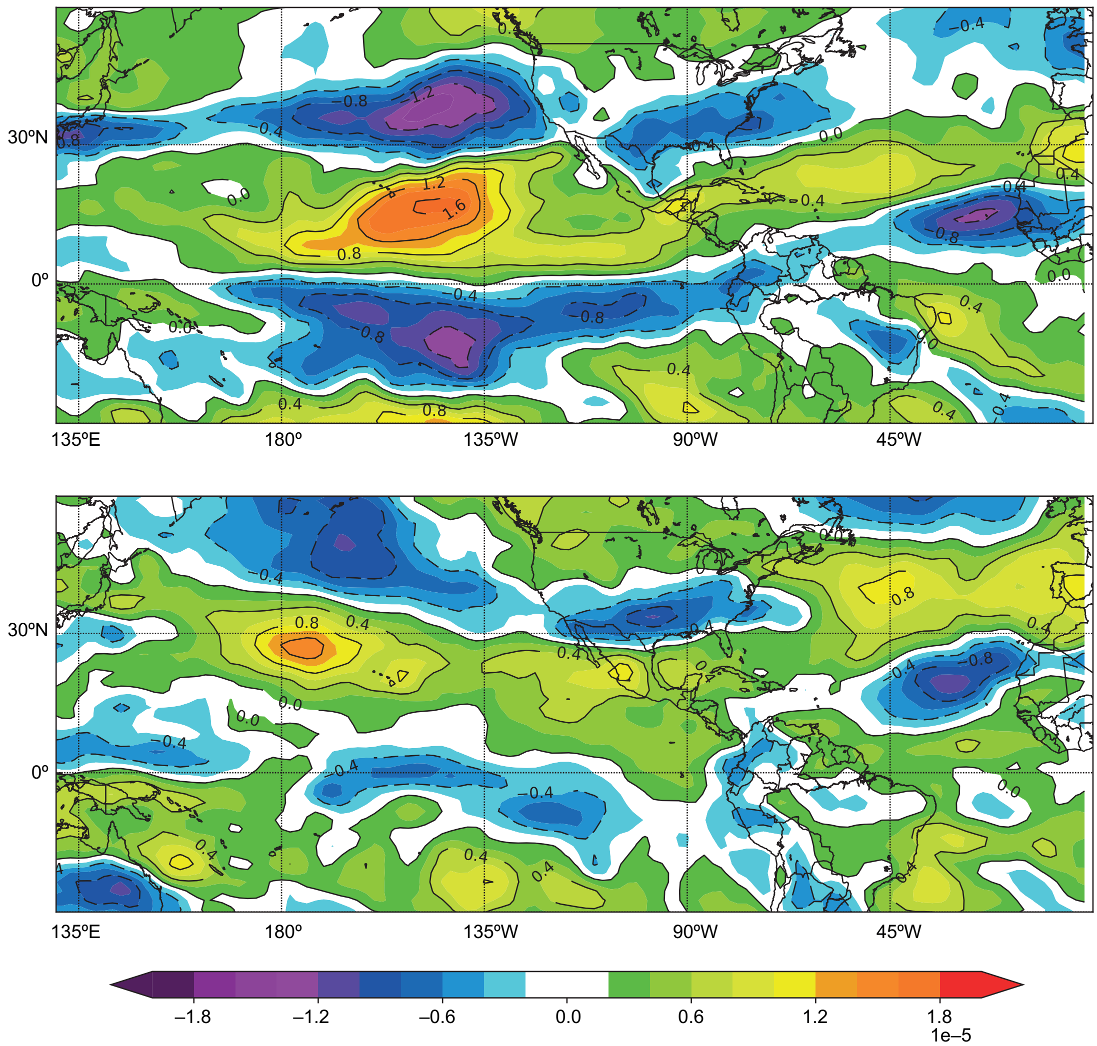

Fig. 10. Composite vorticity at 0.2101 sigma level (s^{-1}) anomalies for CP La Niña (top) and EP La Niño (bottom). Data source: NCEP/NCAR Reanalysis-1 Climatology: 1991-2020.

the basin. Other authors have even determined that in ENSO events the correlation between the Pacific and Tropical Atlantic SSTs is not significant, especially during the boreal winter (Fang and Yu, 2020; Wu et al., 2020); furthermore, it would not offer a clear reason for the non-linearity obtained in some cases. So, this mechanism to explain teleconnection has recently lost support or, for now, continues to require validation.

Figures 4 and 5 of wind anomalies also allow us to analyze another physical process. It was mentioned in the introduction that another proposed mechanism for the ENSO/NAO connection considers that during ENSO, an atypical ridge is configured in the Pacific North America pattern(PNA). This low-frequency ridge would favor the propagation of synoptic-scale wave packets towards the equator, and by the conservation of potential vorticity it would generate an increase in local vorticity; consequently, there will be an increase of the anticyclonic movement until it breaks the wave, which alters the dynamics of the pressure field over the North Atlantic (Graf and Zanchettin, 2012). Figures 4 and 5 show that the scenario best matches this description is La Niña CP, as it presents anomalies in the direction of the rotation over the North Atlantic that correspond

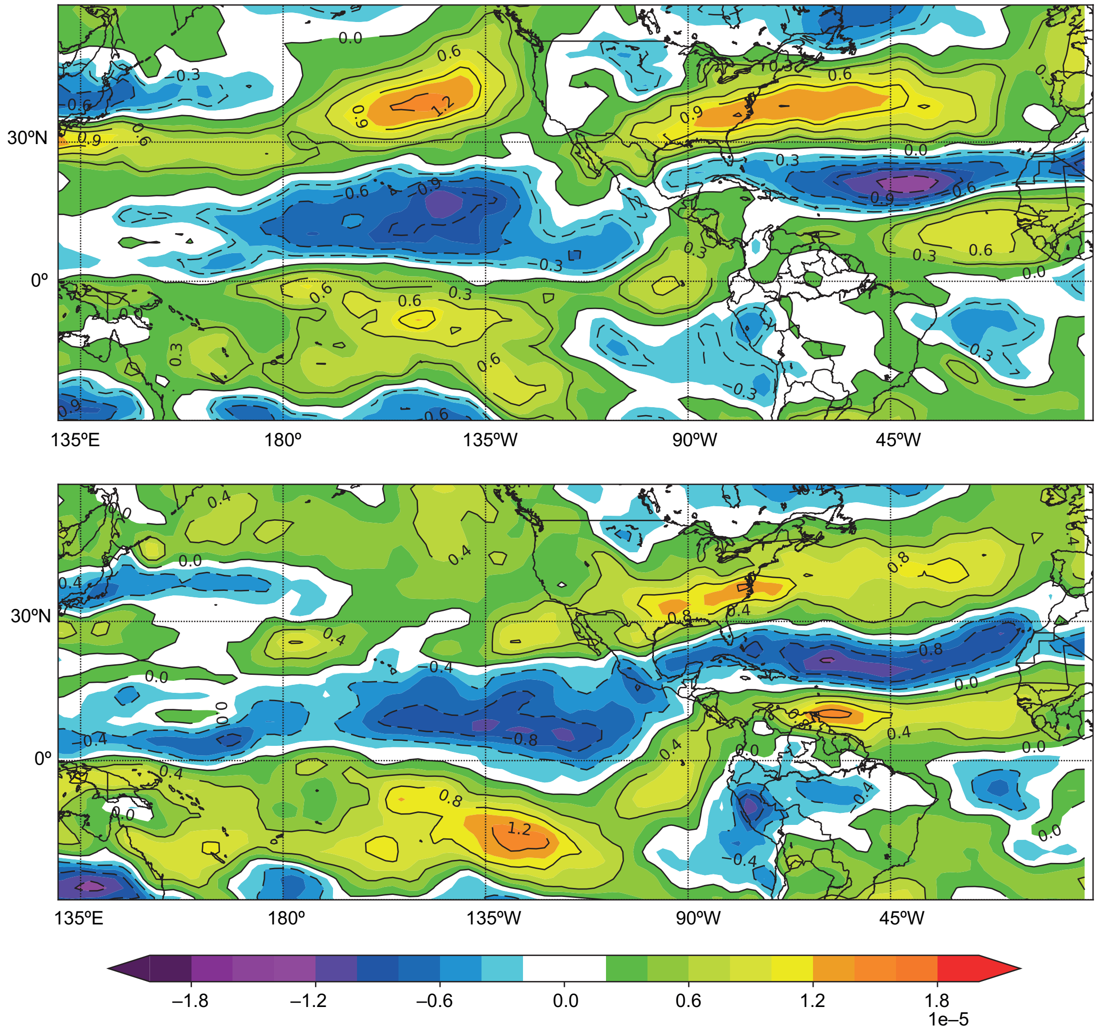

Fig. 11. Composite vorticity at 0.2101 sigma level (s^{-1}) anomalies for CP El Niño (top) and EP El Niño (bottom). Data source: NCEP/NCAR Reanalysis-1 Climatology: 1991-2020.

to the proposed mechanism, which would then be activated for this type of event. It also coincides with the findings of works that link CP La Niña with NAO+ (Zhang et al., 2018), which is precisely the phase corresponding to an increase in anticyclonic movements over this region of the planet. However, it is unclear if this mechanism is also present in the other three cases and how much it could contribute to teleconnection, especially considering that it favors only the positive phase of NAO.

Figures 8 and 9 showing ORL anomalies also reflect some features of the basins' teleconnection. Firstly, CP and EP El Niño tend to generate very similar patterns in the spatial distribution and values of the anomalies. On the contrary, for La Niña cases, the patterns are different, thus supporting the results of this double linear and non-linear dependency, with non-linearity being more evident in La Niña cases.

The impact of ENSO on the behavior of hydroclimatological variables around the planet still needs to be fully understood, since this is essential to improve the predictive capacity and preparedness for possible adverse effects. The estimation of linear correlations has been, from the beginning, the main way to explore the connection between indicators associated to ENSO and its different variables; however, results such as those of the present work show the existence of a non-linear link and the need to design more complex analyses and to propose physical mechanisms that can explain findings such as those described above. The works of Tedeschi et al. (2012, 2016), Navarro-Monterroza et al. (2019), and Wiedermann et al. (2021) have attempted to correlate ENSO with variables such as precipitation, being examples of studies that analyze linear connections; however, even though they found some patterns of causality between ENSO events and anomalies like extreme precipitation events, their authors recognize the difficulty in identifying a relationship that is recurrent for the four possible ENSO scenarios depending on the phase and longitudinal position.

Contributions like that of Tedeschi et al. (2012) aim to identify differences between the impacts on precipitation in South America generated by various SST anomalies over the Pacific. This study found that EP El Niño/La Niña tend to increase/decrease precipitation in the La Plata Basin and, on the contrary, to decrease/increase precipitation over northern South America during all seasons. In the case of CP El Niño/La Niña CP, these typical patterns are not observed, and in some regions the anomalies even show opposite signs. The study used linear correlation analysis, which explains why the results are, in some cases, inconsistent, as the authors state. The added value of the present work is that through the analysis of ENSO-NAO dependence it shows why linear links are insufficient to understand the impact of ENSO types and that the effect of ENSO on the climatic anomalies of different regions may be of a non-linear nature, just as the dynamics of the Pacific and Atlantic seem to be related in a complex way.

The work of Tedeschi et al. (2016) also analyzes the relationship of ENSO in South America with precipitation and its extreme events; in this case, the authors used maps composed of anomalies. This type of analysis allows visualizing the spatial variability generated in each scenario. The results described here are consistent with those described by Tedeschi et al. (2012, 2016) regarding precipitation anomalies, and are complemented with variables such as vorticity and OLR, which show marked differences between CP-type events, and not so defined differences for EP-type events, especially in the cold phase. Another paper exploring the consequences of ENSO on precipitation considering the four modes is that of Navarro-Monterroza et al. (2019), which also estimates linear order correlations without exploring methodologies that consider connections of greater complexity, such as those that seemingly link ENSO and NAO.

Finally, a more recent example of a research incorporating different methods is that of Wiedermann et al. (2021), whose authors highlight that assuming linear statistical dependencies of different ENSO modes with regional climate anomalies does not necessarily seem a justified assumption. In particular, they performed a co-occurrence analysis to determine differences between the spatial scales that present coincidences between ENSO types. They managed to identify that EP periods offer statistically significant rates of the coincidence of events with hydrometeorological anomalies at larger spatial scales, while more dispersed patterns appear in CP periods. These results reveal distinctions in the response to each event around the planet, i.e., not all CP or EP ENSO events will have a unique response precisely because of the complex nature of the climatic teleconnections. As shown in previous studies, it is clear that the influence and impacts of ENSO should be addressed considering their diversity (Ashok and Yamagata, 2009; Takahashi et al., 2011; Feng et al., 2019; Cai et al., 2020).

4. Conclusions

For the NAO and ENSO association, the lowest R coefficients for all cases were observed when every year was considered. For all the cases analyzed, which than include the ENSO years events has the highest R coefficients, that is, when the years with EP La Niña events are omitted, the linear correlation coefficients increase. This can be interpreted as a sign of the nonlinearity in the ENSO/NAO relationship. Of all the indices considered, TNI-NAO relationship exhibited the highest R coefficients, followed by NAO-El Niño 4; on the contrary, NAO-El Niño 1+2 and NAO-El Niño3 showed the lowest coefficients. TNI is an index that represent the gradient of the SST in the Pacific and can represent better its variability. Anomalies maps show that the impact of conditions in the Pacific is different to that in the North Atlantic, especially for the wind, whose anomalies for EP La Niña are the opposite to those of CP La Niña.

Similarly, deep convection is proposed as the mechanism that triggers the atmospheric response and vorticity that modulates energy transport between the Pacific and the North Atlantic.

The maps also showed that the differences in teleconnection can be observed not just for the North Atlantic, and that the anomalies associated to El Niño or La Niña events have several contrasts in the Eastern Pacific and continental territories according to the position of SST anomalies, as validated before. The present study is a continuation of the current efforts to understand the mechanisms and nature of the ENSO/NAO teleconnection with the aim of highlighting the importance of including longitudinal location of ENSO anomalies into seasonal prediction models.

References

Alexander MA, Bladé I, Newman M, Lanzante JR, Lau NC, Scott JD. 2002. The atmospheric bridge: The influence of enso teleconnections on air-sea interaction over the global oceans. Journal of Climate 15: 2205-2231. https://doi.org/10.1175/1520-0442(2002)015<2205:TABTIO>2.0.CO;2

Ashok K, Behera SK, Rao SA, Weng H, Yamagata T. 2007. El Niño Modoki and its possible teleconnection. Journal of Geophysical Research: Oceans 112: C11. https://doi.org/10.1029/2006JC003798

Ashok K, Yamagata T. 2009. The El Niño with a difference. Nature 461: 481-484. https://doi.org/10.1038/461481a

Beltrán L, Díaz DC. 2020. Oscilaciones macroclimáticas que afectan la oferta hídrica en la cuenca del río Gachaneca; Boyacá-Colombia. Revista Brasileira de Meteorologia 35: 171-185. https://doi.org/10.1590/0102-7786351012.

Cai W, McPhaden MJ, Grimm A, Rodrigues R, Taschetto A, Garreaud R, Dewitte B, Germán P, Ham Y-G, Santoso A, Ng B, Anderson W, Wang G, Geng T, Jo H-S, Marengo J, Alves L, Osman M, Li S, Vera C. 2020. Climate impacts of the El Niño -Southern Oscillation on South America. Nature Reviews. Earth and Environment 1: 215-231. https://doi.org//10.1038/s43017-020-0040-3

Capotondi A, Wittenberg AT, Newman M, Di Lorenzo E, Yu, JY, Braconnot P, Cole J, Dewitte B, Giese B, Guilyardi E, Jin FF, Karnauskas K, Kirtman B, Lee T, Schneider N, Xue Y, Yeh SW. 2015. Understanding ENSO diversity. Bulletin of the American Meteorological Society 96: 921-938. https://doi.org/10.1175/BAMS-D-13-00117.1

Capotondi A, Wittenberg AT, Kug J, Takahashi K, McPhaden MJ. 2021. ENSO diversity. In: El Niño Southern Oscillation in a changing climate (McPhaden MJ, Santoso A, Cai W, Eds.). American Geophysical Union, Hoboken, 65-86. https://doi.org/10.1002/9781119548164.ch4

Cassou C, Terray L. 2001. Oceanic forcing of the wintertime low-frequency atmospheric variability in the North Atlantic European sector: A study with the ARPEGE model. Journal of Climate 14: 4266-4291. https://doi.org/10.1175/1520-0442(2001)014<4266:OFOTWL>2.0.CO;2

Díaz D, Villegas N. 2015. Correlación canónica entre índices macroclimáticos y variables meteorológicas de superficie en Colombia. Revista U.D.C.A 18: 543-552. https://doi.org/10.31910/rudca.v18.n2.2015.185

Dommenget D, Bayr T, Frauen C. 2013. Analysis of the non-linearity in the pattern and time evolution of El Niño Southern Oscillation. Climate Dynamics 40: 2825-2847. https://doi.org/10.1007/s00382-012-1475-0

Drouard M, Rivière G, Arbogast P. 2015. The link between the North Pacific climate variability and the North Atlantic Oscillation via downstream propagation of synoptic waves. Journal of Climate 28: 3957-3976. https://doi.org/10.1175/jcli-d-14-00552.1

Du X, Hendy I, Hinnov L, Brown E, Schimmelmann A, Pak D. 2020. Interannual southern California precipitation variability during the Common Era and the ENSO teleconnection. Geophysical Research Letters 47: 1-11. https://doi.org/10.1029/2019GL085891

Fang SW, Yu JY. 2020. A control of ENSO transition complexity by Tropical Pacific mean SSTs through tropical-subtropical interaction. Geophysical Research Letters 47: 0-3. https://doi.org/10.1029/2020GL087933.

Feng Y, Chen X, Tung KK. 2019. ENSO diversity and the recent appearance of Central Pacific ENSO. Climate Dynamics 54: 413-433. https://doi.org/10.1007/s00382-019-05005-7

Fereday DR, Chadwick R, Knight JR, Scaife AA. 2020. Tropical rainfall linked to stronger future ENSO-NAO teleconnection in CMIP5 models. Geophysical Research Letters 47: e2020GL088664. https://doi.org/10.1029/2020GL088664

Graf HF, Zanchettin D. 2012. Central Pacific El Niño, the "subtropical bridge," and Eurasian climate. Journal of

Geophysical Research: Atmospheres 117: 1102. https://doi.org/10.1029/2011JD016493

Gutiérrez JM, Cano R, Cofiño AS, Sordo CM. 2004. Redes probabilísticas y neuronales en las ciencias atmosféricas. Monografías del Instituto Nacional de Meteorología, Madrid, España, 279 pp.

Huang B, Thorne PW, Banzon VF, Boyer T, Chepurin G, Lawrimore JH, Menne MJ, Smith TM, Vose RS, Zhang HM. 2017. Extended reconstructed sea surface temperature, v. 5 (ERSSTv5): Upgrades, validations, and intercomparisons. Journal of Climate 30: 8179-8205. https://doi.org/10.1175/JCLI-D-16-0836.1

Jones PD, Jonsson T, Wheeler D. 1997. Extension to the North Atlantic Oscillation using early instrumental pressure observations from Gibraltar and south-west Iceland. International Journal of Climatology 17: 1433-1450. https://doi.org/10.1002/(SICI)1097-0088(19971115)17:13<1433::AID-JOC203>3.0.CO;2-P

Kalnay E, Kanamitsu M, Kistler R, Collins W, Deaven D, Gandin L, Iredell M, Saha S, White G, Woollen J, Zhu Y, Chelliah M, Ebisuzaki W, Higgins W, Janowiak J, Mo KC, Ropelewski C, Wang J, Leetmaa A, Reynolds R, Jenne R, Joseph D. 1996. The NCEP/NCAR 40-year reanalysis project. Bulletin of the American Meteorological Society 77: 437-472. https://doi.org/10.1175/1520-0477(1996)077<0437:TNYRP>2.0.CO;2

Kao HY, Yu JY. 2009. Contrasting Eastern-Pacific and Central-Pacific types of ENSO. Journal of Climate 22: 615-632. https://doi.org/10.1175/2008JCLI2309.1

Kim H-M, Webster PJ, Curry JA. 2009. Impact of shifting patterns of Pacific Ocean warming on North Atlantic tropical cyclones. Science 325: 77-80. https://doi.org/10.1126/science.1174062

Krzywinski M, Altman N. 2013. Points of significance: Significance, P values and t-tests. Nature Methods 10:1041-1042. https://doi.org/10.1038/nmeth.2698

Kug JS, Jin FF, An S. 2009. Two types of El Niño events: Cold tongue El Niño and warm pool El Niño. Journal of Climate 22: 1499-1515. https://doi.org/10.1175/2008JCLI2624.1

Li Y, Lau NC. 2012. Impact of ENSO on the atmospheric variability over the North Atlantic in late winter-role of transient eddies. Journal of Climate 25: 320-342. https://doi.org/10.1175/JCLI-D-11-00037.1

Mohammadi B, Vaheddoost B, Danandeh Mehr A. 2020. A spatiotemporal teleconnection study between Peruvian precipitation and oceanic oscillations. Quaternary International 565: 1-11. https://doi.org/10.1016/j.quaint.2020.09.042

Moron V, Gouirand I. 2003. Seasonal modulation of the El Niño-Southern Oscillation relationship with sea level pressure anomalies over the North Atlantic in October-March 1873-1996. International Journal of Climatology 23: 143-155. https://doi.org/10.1002/JOC.868

Navarro-Monterroza E, Arias PA. Vieira SC. 2019. El Niño-Oscilación del Sur, fase Modoki, y sus efectos en la variabilidad espacio-temporal de la precipitación en Colombia. Revista de la Academia Colombiana de Ciencias Exactas, Físicas y Naturales 43: 120-132. https://doi.org/10.18257/raccefyn.704.

Salas HD, Poveda G, Mesa ÓJ, Marwan N. 2020. Generalized synchronization between ENSO and hydrological variables in Colombia: A recurrence quantification approach. Frontiers in Applied Mathematics and Statistics 6: 1-20. https://doi.org/10.3389/fams.2020.00003

Sullivan A, Luo JJ, Hirst AC, Bi D, Cai W, He J. 2016. Robust contribution of decadal anomalies to the frequency of central-Pacific El Niño. Scientific Reports 6: 1-7. https://doi.org/10.1038/srep38540

Takahashi K, Montecinos A, Goubanova K, Dewitte B. 2011. ENSO regimes: Reinterpreting the canonical and Modoki El Niño. Geophysical Research Letters 38: 1-5. https://doi.org/10.1029/2011GL047364

Tedeschi RG, Cavalcanti, IF, Grimm AM. 2012. Influences of two types of ENSO on South American precipitation. International Journal of Climatology 33: 1382-1400. https://doi.org/10.1002/joc.3519

Tedeschi RG, Grimm AM, Cavalcanti, IFA. 2015. Influence of central and east ENSO on extreme events of precipitation in South America during austral spring and summer. International Journal of Climatology 35: 2045-2064. https://doi.org/10.1002/joc.4106

Tedeschi RG, Grimm AM, Cavalcanti IF. 2016. Influence of central and east ENSO on precipitation and its extreme events in South America during austral autumn and winter. International Journal of Climatology 36: 4797-4814. https://doi.org/10.1002/joc.3519

Visbeck MH, Hurrell JW, Polvani L, Cullen HM. 2001. The North Atlantic Oscillation: Past, present, and future. Proceedings of the National Academy of Sciences of the United States of America 98: 12876-12877. https://doi.org/10.1073/pnas.231391598

Wang C. 2002. Atlantic climate variability and its associated atmospheric circulation cells. Journal of Climate 15: 1516-1536. https://doi.org/10.1175/1520-0442(2002)015<1516:ACVAIA>2.0.CO;2

Wang X, Tan W, Wang C. 2018. A new index for identifying different types of El Niño Modoki events. Climate Dynamics 50: 2753-2765. https://doi.org/10.1007/s00382-017-3769-8

Whan K, Zwiers F. 2017. The impact of ENSO and the NAO on extreme winter precipitation in North America in observations and regional climate models. Climate Dynamics 48: 1401-1411. https://doi.org/10.1007/s00382-016-3148-x

Wiedermann M, Siegmund JF, Donges JF, Donner RV. 2021. Differential imprints of distinct ENSO flavors in global patterns of very low and high seasonal precipitation. Frontiers in Climate 3: 618548. https://doi.org/10.48550/arXiv.1702.00218

Wu R, He Z. 2019. Northern Tropical Atlantic warming in El Niño decaying spring: Impacts of El Niño amplitude. Geophysical Research Letters 46: 14072-14081. https://doi.org/10.1029/2019GL085840

Wu R, Lin M, Sun H. 2020. Impacts of different types of El Niño and La Niña on northern tropical Atlantic sea surface temperature. Climate Dynamics 54: 4147-4167. https://doi.org/10.1007/s00382-020-05220-7

Zhang W, Wang L, Xiang B, Qi L, He J. 2015. Impacts of two types of La Niña on the NAO during boreal winter. Climate Dynamics 44: 1351-1366. https://doi.org/10.1007/s00382-014-2155-z

Zhang W, Wang Z, Stuecker MF, Turner AG, Jin FF, Geng X. 2018. Impact of ENSO longitudinal position on teleconnections to the NAO. Climate Dynamics 52: 257-274. https://doi.org/10.1007/s00382-018-4135-1